

Arbitrarily shaped plates analysis via Line Element-Less Method (LEM)

G. Battaglia¹, A. Di Matteo², G. Micale³, A. Pirrotta^{4,5}

^{1,3}Dipartimento di Ingegneria Civile, Ambientale, Aerospaziale, dei Materiali (DICAM),
Università degli Studi di Palermo, Viale delle Scienze I-90128 Palermo, Italy.

¹*E-mail: giuseppe.battaglia03@unipa.it*

²*E-mail: alberto.dimatteo@unipa.it*

⁴*E-mail: antonina.pirrotta@unipa.it*

³Dipartimento della Innovazione Digitale ed Industriale
Università degli Studi di Palermo, Viale delle Scienze I-90128 Palermo, Italy.

³*E-mail: giorgiod.maria.micale@unipa.it*

⁵Department of Mathematical Sciences
University of Liverpool, Liverpool, UK

⁵*E-mail: antonina.pirrotta@liverpool.ac.uk*

Corresponding author: Prof. Antonina Pirrotta

Keywords: Kirchoff plate; Harmonic Polynomials; Line Element-Less Method; Meshfree method; Arbitrary shape.

Abstract

An innovative procedure is introduced for the analysis of arbitrarily shaped thin plates with various boundary conditions and under generic transverse loading conditions. Framed into Line Element-less Method, a truly meshfree method, this novel approach yields the solution in terms of the deflection function in a straightforward manner, without resorting to any discretization, neither in the domain nor on the boundary. Specifically, expressing the deflection function through a series expansion in terms of harmonic polynomials, it is shown that the proposed method requires only the evaluation of line integrals along the boundary parametric equation. Further, minimization of appropriately introduced novel functionals directly leads to simple systems of linear algebraic equations for the unknown expansion coefficients. Notably, the proposed procedure yields exact solutions, when available, for different plate geometries. Additionally, several numerical applications are presented to show the reliability and simplicity of the approach, and comparisons with pertinent Finite Element method data demonstrate the efficiency and accuracy of the proposed procedure.

1 Introduction

Many structural problems in engineering mechanics are governed by partial differential equations (PDEs) whose exact solutions is known for few restricted cases of practical interest. In this regard, the evaluation of the structural response of plates under generic loading conditions, commonly described via a biharmonic PDE in Kirchoff's theory, is a well-established problem in applied mechanics due to the constant use of these structural elements in most engineering fields.

Clearly, since exact plate solutions are available only for certain shapes, boundary and loading conditions [1], several numerical procedures have been proposed and their development still attracts the attentions of many researchers in the field [2-4]. In this context, the Finite Element Method (FEM) [5] and Boundary Element Method (BEM) [6] unquestionably represent the most commonly employed and powerful numerical techniques for general structural analysis.

As well-known the use of mesh, be it in the domain or in the boundary, is a common characteristic of these traditional approaches. Specifically, while conventional FEM approach basically requires a discretization over the entire domain through finite elements mesh, in the BEM an integral equation is obtained and a boundary mesh is required to numerically approximate the boundary integrals involved. It is worth underscoring that, in this latter approach the governing differential equation is satisfied exactly inside the domain and high accuracy is generally achieved with a relatively small number of boundary elements. Notably, the extensive research efforts devoted in the last few decades to the development of these approaches have allowed to circumvent most numerical problems associated to the domain or boundary discretization, thus making FEM and BEM the dominant approaches for most problems in computational mechanics.

Nevertheless, the possibility of obtaining numerical solutions for PDEs without resorting to any discretization, that is the so-called meshless approach, has rather recently gained the attention of scientists and engineers working in this field. As defined in [7] a meshless method, also referred to as meshfree method, is a method used to establish system equations for the whole problem domain without the use of a predefined mesh for the domain discretization. This approach has, therefore, become an alternative to classical FEM and BEM due to some beneficial features such as its flexibility, wide applicability and the possibility of avoiding problems related to meshing and remeshing in the domain or boundary [7, 8].

In this regard, framed in the meshless approach, different procedures have been proposed to solve a variety of engineering problems [9], such as the element free Galerkin Method [10, 11], Petrov–Galerkin approach [12], h-p clouds method [13], and the reproducing kernel element method [14] among the others. Further, specifically referring to the plate analysis, the works in [15-22] and references therein can be mentioned. Finally, note that other classes of methods, which are

inherently meshless, exist for the plate bending problem, including the Trefftz method [23], the pb-2 Rayleigh-Ritz method [24, 25], and the Galerkin method [26].

Additionally, a novel truly meshless procedure, namely the Line Element-less Method (LEM), has been introduced for the analysis of De Saint Venant pure torsion and flexure-torsion problem for both isotropic and orthotropic material [27-31]. Notably, this method does not require any discretization neither in the domain nor on the boundary, and all the involved integrals are simple line integrals. Further, based on the analogy between plates bending under edge moments and beams in torsion [32-34], recently the aforementioned LEM has been employed for the bending problem of simply supported plates subject to uniformly distributed edge moments [35].

In this context, aim of this paper is to extend the LEM for the analysis of arbitrarily shaped plates, without any holes, assuming various boundary conditions (BCs) and subject to transverse loads. Specifically, the original biharmonic PDE, which rules the plate deflection, is decomposed in two Poisson's equations, whose solution is expressed as the superposition of pertinent particular solution and harmonic polynomials with unknown expansion coefficients. These coefficients are then determined satisfying the prescribed BCs on the contour.

Note that, in the proposed procedure the BCs are satisfied in a least square sense on the plate contour, and only line integrals along the boundary parametric equation are required, leading to systems of linear algebraic equations for the unknown expansion coefficients.

Remarkably, as it will be shown in the following, this procedure yields exact closed-form solutions when available, for different plates geometries, while in the other cases approximate accurate analytical solutions are achieved generally employing few terms in the series expansion. This may be clearly considered an attractive feature of the proposed method, especially with respect to other meshfree procedure which are inherently exclusively numerical in nature.

Interestingly, unlike the Trefftz method [23], where the BCs are enforced in a number of boundary points to determine pertinent expansion coefficients, or classical meshfree approaches, where several nodes are generally considered in the domain, this proposed procedure is entirely element-free. Further, with respect to the classical Rayleigh-Ritz approach [24, 25] more general plate shapes and BCs can be handled, and cumbersome integration over domains are not involved. These aspects may clearly represent an advantage of the proposed procedure.

Several numerical applications will be shown, demonstrating the elegance and simplicity of the proposed procedure, and corresponding data vis-à-vis classical FEM results will be reported, assessing the accuracy and reliability of the procedure.

2 Problem definition

Consider a homogeneous isotropic thin plate, of arbitrary shape with contour Γ and domain Ω , uniform thickness h and modulus of elasticity E , generally referred to as Kirchhoff plate (see Fig. 1). The governing differential equation in terms of transverse deflection $w(x, y)$ is the well-known biharmonic equation [1, 36]

$$\left(\frac{\partial^2}{\partial x^2} + \frac{\partial^2}{\partial y^2} \right) \left(\frac{\partial^2 w}{\partial x^2} + \frac{\partial^2 w}{\partial y^2} \right) = \frac{q(x, y)}{D} \quad (1)$$

where $q(x, y)$ is the transverse distributed load, $D = Eh^3/12(1-\nu^2)$ is the flexural rigidity of the plate and ν is the Poisson ratio.

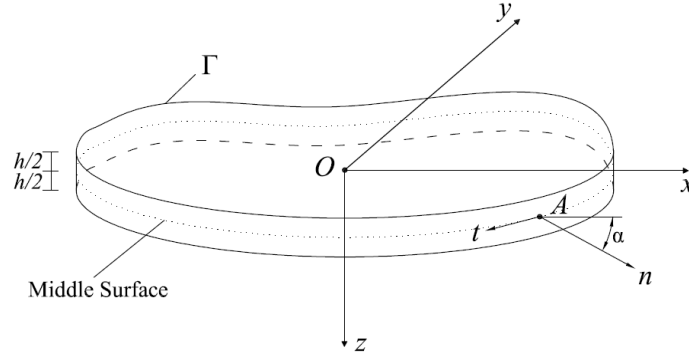


Fig. 1 Plate with arbitrary shape

The bending moments $M_x(x, y)$ and $M_y(x, y)$, and the twisting moment $M_{xy}(x, y)$ are given as

$$M_x(x, y) = -D \left(\frac{\partial^2 w}{\partial x^2} + \nu \frac{\partial^2 w}{\partial y^2} \right) \quad (2.a)$$

$$M_y(x, y) = -D \left(\frac{\partial^2 w}{\partial y^2} + \nu \frac{\partial^2 w}{\partial x^2} \right) \quad (2.b)$$

$$M_{xy}(x, y) = -D(1-\nu) \frac{\partial^2 w}{\partial x \partial y} \quad (2.c)$$

while the shearing forces $V_x(x, y)$ and $V_y(x, y)$ are given by

$$V_x(x, y) = -D \frac{\partial}{\partial x} \left(\frac{\partial^2 w}{\partial x^2} + \frac{\partial^2 w}{\partial y^2} \right) \quad (3.a)$$

$$V_y(x, y) = -D \frac{\partial}{\partial y} \left(\frac{\partial^2 w}{\partial x^2} + \frac{\partial^2 w}{\partial y^2} \right) \quad (3.b)$$

Further, introducing the so-called moment sum $M(x, y)$ as

$$M(x, y) = \frac{M_x + M_y}{1 + \nu} \quad (4)$$

Eq. (1) can be recast into two equivalent Poisson's equations as [37]

$$\nabla^2 M(x, y) = -q(x, y) \quad (5.a)$$

and

$$\nabla^2 w(x, y) = -\frac{M(x, y)}{D} \quad (5.b)$$

where $\nabla^2(\cdot) = \frac{\partial^2(\cdot)}{\partial x^2} + \frac{\partial^2(\cdot)}{\partial y^2}$ is the well-known Laplace operator.

Thus, the solution of the plate problem Eq. (1) reduces to the integration of the two Eqs. (5 a, b) in succession, which is sometimes preferred depending upon the method of solution employed.

As far as the boundary conditions (BCs) are concerned, denote as n and t the outward unit normal and tangent vector at a point A of a generic curvilinear edge of the contour Γ , and let α be the angle between the normal n and the x axis (see Fig. 1). Thus, for the most common cases, the boundary conditions for the curvilinear edge can be specified as [38-40]

i. Simply-supported edge

$$w(x, y) = 0 \quad (6.a)$$

$$M_n(x, y) = 0 \quad (6.b)$$

where $M_n(x, y)$ denotes the normal bending moment applied at the edge, and is given as

$$M_n(x, y) = n_x^2 M_x + n_y^2 M_y + 2n_x n_y M_{xy} \quad (7)$$

where n_x and n_y are the components of the unitary vector n along the x and y axes, respectively.

Note that, considering Eqs. (2) and (7), Eq. (6.b) becomes

$$\left(n_x^2 + \nu n_y^2\right) \frac{\partial^2 w}{\partial x^2} + 2(1 - \nu)n_x n_y \frac{\partial^2 w}{\partial x \partial y} + \left(n_y^2 + \nu n_x^2\right) \frac{\partial^2 w}{\partial y^2} = 0 \quad (8)$$

ii. Clamped edge

$$w(x, y) = 0 \quad (9.a)$$

$$\frac{\partial w(x, y)}{\partial n} = n_x \frac{\partial w}{\partial x} + n_y \frac{\partial w}{\partial y} = 0 \quad (9.b)$$

iii. Free edge

$$M_n(x, y) = 0 \quad (10.a)$$

$$\tilde{V}_n = V_n + \frac{\partial M_{nt}}{\partial s} = 0 \quad (10.b)$$

where $\tilde{V}_n(x, y)$ is the so-called effective shear force, while $M_{nt}(x, y)$ and $V_n(x, y)$ represent the twisting moment and the shearing force on the edge of the plate, and are given as

$$M_{nt}(x, y) = (n_x^2 + n_y^2)M_{xy} + n_x n_y (M_y - M_x) \quad (11)$$

and

$$V_n(x, y) = n_x V_x + n_y V_y \quad (12)$$

Clearly, taking into account Eqs. (2, 3) and Eqs. (11, 12), the condition in Eq. (10.b) can be expressed in terms of the transverse deflection $w(x, y)$.

Notably, the above reported BCs considerably simplify in case of straight edges [36]. For instance, for an edge parallel to the y axis Eq. (10.b) can be directly given as

$$\frac{\partial^3 w}{\partial x^3} + (2 - \nu) \frac{\partial^3 w}{\partial x \partial y^2} = 0 \quad (13)$$

3 Line Element-Less Method for plate analysis

In this section LEM approach is introduced for the analysis of arbitrary shaped plates, without holes, with general BCs and under a transverse load $q(x, y)$. Specifically, based on the classical applications of the LEM [27-31] and taking into account Eqs. (5), $M(x, y)$ and $w(x, y)$ can be expressed in terms of the so-called harmonic polynomials P_k and Q_k , generally defined as

$$P_k(x, y) = \text{Re}(x + iy)^k \quad (14.a)$$

$$Q_k(x, y) = \text{Im}(x + iy)^k \quad (14.b)$$

or, recursively as

$$P_k(x, y) = P_{k-1}x - Q_{k-1}y \quad (15.a)$$

$$Q_k(x, y) = Q_{k-1}x - P_{k-1}y \quad (15.b)$$

which are valid for $k > 0$, and with $P_0 = 1$ and $Q_0 = 0$.

Further, the derivatives of the harmonic polynomials are

$$\frac{\partial P_k}{\partial x} = kP_{k-1}; \quad \frac{\partial P_k}{\partial y} = -kQ_{k-1} \quad (16.a)$$

$$\frac{\partial Q_k}{\partial x} = kQ_{k-1}; \quad \frac{\partial Q_k}{\partial y} = kP_{k-1} \quad (16.b)$$

$$\nabla^2 P_k = 0; \nabla^2 Q_k = 0 \quad \forall k \quad (16.c)$$

Based on the above relations, it can be argued that a solution of Eq. (5.a) can be obtained expressing the moment sum function as the sum of harmonic polynomials, which satisfy the Laplace equation as in Eq. (16.c), and a particular solution of the Poisson equation Eq. (5.a), namely $M_p(x, y)$; that is

$$M(x, y) = \sum_{k=0}^n a_k P_k(x, y) + \sum_{k=1}^n b_k Q_k(x, y) + M_p(x, y) \quad (17)$$

where a_k and b_k are $(2n+1)$ unknown coefficients to be determined, and n is an integer number which denotes the truncation limit of the series expansion.

Further, introducing the vectors

$$\mathbf{p}_n(x, y) = \begin{bmatrix} P_0(x, y) \\ \vdots \\ P_n(x, y) \end{bmatrix}; \quad \mathbf{q}_n(x, y) = \begin{bmatrix} Q_1(x, y) \\ \vdots \\ Q_n(x, y) \end{bmatrix}; \quad \mathbf{a} = \begin{bmatrix} a_0 \\ \vdots \\ a_n \end{bmatrix}; \quad \mathbf{b} = \begin{bmatrix} b_1 \\ \vdots \\ b_n \end{bmatrix} \quad (18)$$

Eq. (17) can conveniently be rewritten in compact form as

$$M(x, y) = \mathbf{r}_n \boldsymbol{\eta} + M_p(x, y) \quad (19)$$

where

$$\mathbf{r}_n = \begin{bmatrix} \mathbf{p}_n^T & \mathbf{q}_n^T \end{bmatrix}; \quad \boldsymbol{\eta} = \begin{bmatrix} \mathbf{a} \\ \mathbf{b} \end{bmatrix} \quad (20)$$

are the vector containing the harmonic polynomials and the unknown coefficients, respectively.

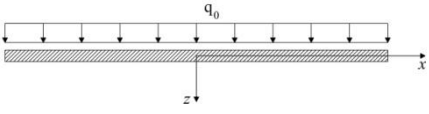
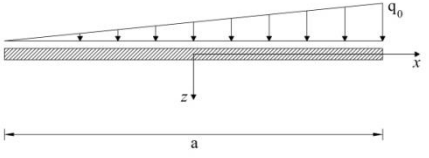
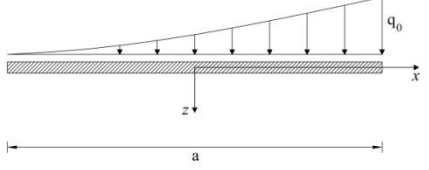
Note that, as far as the particular solution $M_p(x, y)$ of Eq. (5.a) is concerned, this can be obtained in closed-form using the approach in [41] (see Appendix A) when the load function $q(x, y)$ is represented by a homogeneous polynomial of degree N ; i.e.

$$q(x, y) = \sum_{k=0}^N A_k x^{N-k} y^k \quad (21)$$

where A_k are known coefficients which depend on the form of the assigned load. For completeness sake, expressions of $M_p(x, y)$ are reported in Tab. 1 for some common cases of transverse distributed load $q(x, y)$. Further, as suggested in [42], if the function $q(x, y)$ is not directly given in the form of Eq. (21), it can be initially approximated by a truncated series of Chebyshev polynomials which can be recast in the form of Eq. (21). Clearly, this yields a quite versatile tool for expressing various shapes of load distributions, and even concentrated loads, as it will be shown in the following section.

As far as the unknown coefficients in Eq. (17) or (19) are concerned, the $(2n+1)$ values of a_k and b_k in the vector $\boldsymbol{\eta}$ can be determined appropriately imposing the specified BCs of the plate. In this context, it is convenient to firstly consider the simplified case of polygonal plate with simply-supported edges, which will be then further generalized to arbitrary shaped plates with any boundary conditions.

Tab. 1. Particular solution of Eq. (5.a) for different distributed loads

| Type of load | Load function | Particular solution |
|---|---|---|
| <p style="text-align: center;"><i>Uniform</i></p>  | $q(x, y) = q_0$ | $M_p(x, y) = -\frac{q_0}{4}(x^2 + y^2)$ |
| <p style="text-align: center;"><i>Triangular</i></p>  | $q(x, y) = q_0 \left(\frac{1}{2} + \frac{x}{a} \right)$ | $M_p(x, y) = -\frac{q_0}{2} \left(\frac{x^2}{2} + \frac{x^3}{3a} \right)$ |
| <p style="text-align: center;"><i>Parabolic</i></p>  | $q(x, y) = \frac{q_0}{a^2} \left(x^2 + ax + \frac{a^2}{4} \right)$ | $M_p(x, y) = -\frac{q_0}{2} \left(\frac{x^2}{4} + \frac{x^3}{3a} + \frac{x^4}{6a^2} \right)$ |

3.1 Simply-supported polygonal plate

Let the plate be of polygonal shape and with all the edges simply-supported. Since in this case the moment sum function must be zero along the entire contour of the polygonal plate [32, 35], the following relation holds

$$M_n(x, y) = M(x, y) = 0, \quad \text{in } \Gamma \quad (22)$$

Taking into account Eq. (22), it is feasible to evaluate these unknown coefficients $\boldsymbol{\eta}$ in Eq. (19) applying a minimization procedure on the closed contour path integral of the squared moment sum function

$$\Psi(\boldsymbol{\eta}) = \oint_{\Gamma} [M(x, y)]^2 d\gamma \quad (23)$$

Thus, introducing Eq. (19) into Eq. (23), the functional can be recast as

$$\Psi(\boldsymbol{\eta}) = \oint_{\Gamma} \left[(\mathbf{r}_n \boldsymbol{\eta})^2 + M_p^2(x, y) + 2\mathbf{r}_n \boldsymbol{\eta} M_p(x, y) \right] d\gamma \quad (24)$$

Further, performing variations of the above functional with respect to $\boldsymbol{\eta}$, yields

$$\frac{\partial \Psi(\boldsymbol{\eta})}{\partial \boldsymbol{\eta}} = \mathbf{Q}_n \boldsymbol{\eta} + \boldsymbol{\tau} = \mathbf{0} \quad (25)$$

which is a linear algebraic system in the unknowns $\boldsymbol{\eta}$, where

$$\mathbf{Q}_n = 2 \oint_{\Gamma} \mathbf{r}_n^T \mathbf{r}_n d\gamma \quad (26.a)$$

$$\boldsymbol{\tau} = 2 \oint_{\Gamma} \mathbf{r}_n^T M_p(x, y) d\gamma \quad (26.b)$$

In this manner the vector $\boldsymbol{\eta}$ can be directly evaluated as

$$\boldsymbol{\eta} = -\mathbf{Q}_n^{-1} \boldsymbol{\tau} \quad (27)$$

and, taking into account Eq. (19), the moment sum function can be expressed as

$$M(x, y) = -\mathbf{r}_n \mathbf{Q}_n^{-1} \boldsymbol{\tau} + M_p(x, y) \quad (28)$$

Once $M(x, y)$ is determined, the deflection function $w(x, y)$ can be obtained solving Eq. (5.b).

Specifically, as similarly done for the moment sum function, a solution of Eq. (5.b) can be sought assuming $w(x, y)$ as the sum of harmonic polynomials, and a particular solution of the Poisson equation Eq. (5.b), namely $w_p(x, y)$; that is

$$w(x, y) = \sum_{k=0}^m c_k P_k(x, y) + \sum_{k=1}^m d_k Q_k(x, y) + w_p(x, y) \quad (29)$$

where c_k and d_k are $(2m+1)$ unknown coefficients to be determined, and m is an integer number which denotes the truncation limit of the series expansion.

Again, note that the particular solution $w_p(x, y)$ can be evaluated applying the procedure in Appendix A considering the obtained moment sum function $M(x, y)$ in Eq. (28).

As far as the unknown coefficients in Eq. (29) are concerned, the $(2m+1)$ values of c_k and d_k are determined appropriately imposing the BCs. In this regard, Eq. (29) can conveniently be rewritten in compact form as

$$w(x, y) = \mathbf{r}_m \boldsymbol{\xi} + w_p(x, y) \quad (30)$$

where $\boldsymbol{\xi}^T = [\mathbf{c}^T \quad \mathbf{d}^T]$ is the vector containing the unknown coefficients, and

$$\mathbf{r}_m = [\mathbf{p}_m^T \quad \mathbf{q}_m^T]; \quad \mathbf{p}_m(x, y) = \begin{bmatrix} P_0(x, y) \\ \vdots \\ P_m(x, y) \end{bmatrix}; \quad \mathbf{q}_m(x, y) = \begin{bmatrix} Q_1(x, y) \\ \vdots \\ Q_m(x, y) \end{bmatrix}; \quad \mathbf{c} = \begin{bmatrix} c_0 \\ \vdots \\ c_m \end{bmatrix}; \quad \mathbf{d} = \begin{bmatrix} d_1 \\ \vdots \\ d_m \end{bmatrix} \quad (31)$$

Therefore, considering that for a simply-supported plate Eq. (6.a) holds, the vector ξ can be found minimising the closed contour path integral of the squared deflection function; that is

$$\Theta(\xi) = \oint_{\Gamma} [w(x, y)]^2 d\gamma \quad (32)$$

Introducing Eq. (30) into Eq. (32), and performing variation with respect to the unknown coefficients leads to an algebraic linear system in terms of the unknowns ξ , as

$$\frac{\partial \Theta(\xi)}{\partial \xi} = \mathbf{Q}_m \xi + \lambda = \mathbf{0} \quad (33)$$

where

$$\mathbf{Q}_m = 2 \oint_{\Gamma} \mathbf{r}_m^T \mathbf{r}_m d\gamma \quad (34.a)$$

$$\lambda = 2 \oint_{\Gamma} \mathbf{r}_m^T w_p(x, y) d\gamma \quad (34.b)$$

Finally, obtaining the vector ξ from Eq. (33) as

$$\xi = -\mathbf{Q}_m^{-1} \lambda \quad (35)$$

and substituting in Eq. (30), yields the sought deflection function of the plate $w(x, y)$ as

$$w(x, y) = -\mathbf{r}_m \mathbf{Q}_m^{-1} \lambda + w_p(x, y) \quad (36)$$

Note that if the number of terms in Eq. (29) corresponds to the one in Eq. (17), that is if $n = m$, then $\mathbf{r}_m = \mathbf{r}_n$ and $\mathbf{Q}_m = \mathbf{Q}_n$; thus in this case it is only necessary to compute \mathbf{Q}_n via Eq. (27.a) once beforehand.

3.2 General plate analysis

As previously mentioned, the above discussed procedure is strictly valid for polygonal plates with all edges simply-supported. In this case, in fact, both the moment sum and the deflection functions must be null on the contour, that is $M(x, y) = 0$ and $w(x, y) = 0$ in Γ . Notably, these properties allow the functionals $\Psi(\boldsymbol{\eta})$ and $\Theta(\xi)$ to be expressed as in Eqs. (23) and (32), respectively.

Clearly, in the generic case of arbitrarily shaped plates with any BCs, neither $M(x, y)$ nor $w(x, y)$ equal zero on the entire contour, and hence Eqs. (27, 35) cannot be directly used to find the unknown coefficients. This is, for instance, the case of a plate with curved

boundaries ($M(x, y) \neq 0$ in Γ), in which at least one edge can undergo vertical deflections ($w(x, y) \neq 0$ in Γ). Therefore, the possibility of the moment sum or the deflection functions not to vanish in Γ should be appropriately accounted for in the evaluation of the unknown coefficients.

In this regard, assuming that the plate boundary conditions are the same on the entire contour Γ , the functional in Eq. (23) can be properly modified as

$$\tilde{\Psi}(\boldsymbol{\eta}) = \oint_{\Gamma} [M(x, y) - \tilde{M}(x, y)]^2 d\gamma \quad (37)$$

where $M(x, y)$ is given in Eq. (17) and $\tilde{M}(x, y)$ is an additional function, conveniently introduced to take into account the generic plate boundary conditions. As apparent from Eq. (37), this function represents the pertinent moment sum function evaluated on the boundary. For consistency, $\tilde{M}(x, y)$ can be expressed in terms of harmonic polynomials as

$$\tilde{M}(x, y) = \sum_{k=0}^{\tilde{n}} \tilde{a}_k P_k(x, y) + \sum_{k=1}^{\tilde{n}} \tilde{b}_k Q_k(x, y) \quad (38)$$

in which \tilde{a}_k and \tilde{b}_k are unknown coefficients to be determined, while \tilde{n} is an integer number denoting the truncation limit of the series expansion, with $\tilde{n} < n$ and generally small.

Denoting as

$$\mathbf{p}_{\tilde{n}}(x, y) = \begin{bmatrix} P_0(x, y) \\ \vdots \\ P_{\tilde{n}}(x, y) \end{bmatrix}; \quad \mathbf{q}_{\tilde{n}}(x, y) = \begin{bmatrix} Q_1(x, y) \\ \vdots \\ Q_{\tilde{n}}(x, y) \end{bmatrix}; \quad \tilde{\mathbf{a}} = \begin{bmatrix} \tilde{a}_0 \\ \vdots \\ \tilde{a}_{\tilde{n}} \end{bmatrix}; \quad \tilde{\mathbf{b}} = \begin{bmatrix} \tilde{b}_1 \\ \vdots \\ \tilde{b}_{\tilde{n}} \end{bmatrix} \quad (39)$$

Eq. (38) can conveniently be rewritten in compact form as

$$\tilde{M}(x, y) = \mathbf{s}_{\tilde{n}} \tilde{\boldsymbol{\eta}} \quad (40)$$

where

$$\mathbf{s}_{\tilde{n}} = \begin{bmatrix} \mathbf{p}_{\tilde{n}}^T & \mathbf{q}_{\tilde{n}}^T \end{bmatrix}; \quad \tilde{\boldsymbol{\eta}} = \begin{bmatrix} \tilde{\mathbf{a}} \\ \tilde{\mathbf{b}} \end{bmatrix} \quad (41)$$

Clearly, as shown in Fig. 2 if the plate BCs vary on the contour Γ , it is feasible to appropriately subdivide Γ in the N_{γ} edges Γ_i on which the BCs remain constant, that is $\Gamma = \bigcup_{i=1}^{N_{\gamma}} \Gamma_i$.

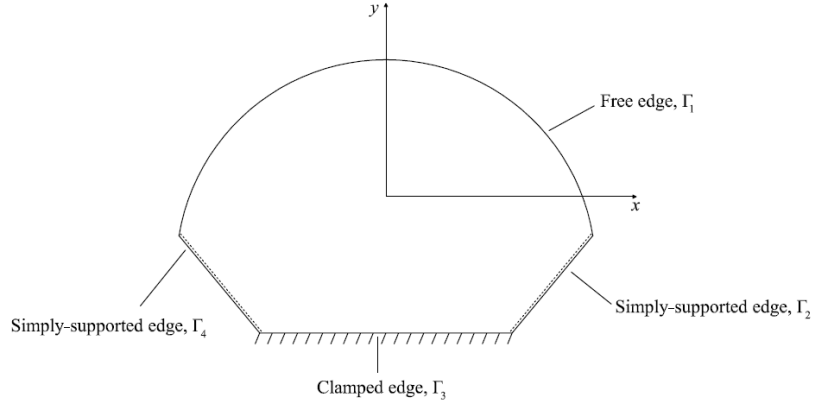


Fig. 2 Arbitrary shaped plate with mixed BCs and $N_\gamma = 4$.

Therefore, the functional in Eq. (37) becomes

$$\tilde{\Psi}(\boldsymbol{\eta}) = \sum_{i=1}^{N_\gamma} \int_{\Gamma_i} [M(x, y) - \tilde{M}_i(x, y)]^2 d\gamma \quad (42)$$

where the symbol $\int_{\Gamma_i} (\cdot) d\gamma$ denotes the classical line integration and, similarly to Eq. (40), the

function $\tilde{M}_i(x, y)$, representing the moment sum function on the corresponding edge, is given by

$$\tilde{M}_i(x, y) = \mathbf{s}_n \tilde{\boldsymbol{\eta}}_i; \quad i = 1, \dots, N_\gamma \quad (44)$$

where the subscript i refers to the i -th edge Γ_i . It is worth stressing that, as previously mentioned, $\tilde{M}_i(x, y)$ equals zero only for simply-supported straight edges.

Taking into account Eqs. (19) and (44) and substituting in Eq. (42), yields

$$\tilde{\Psi}(\boldsymbol{\eta}) = \sum_{i=1}^{N_\gamma} \int_{\Gamma_i} [\mathbf{r}_n \boldsymbol{\eta} + M_p(x, y) - \mathbf{s}_n \tilde{\boldsymbol{\eta}}_i]^2 d\gamma \quad (45)$$

Analogously, to allow for the possibility of vertical deflections on the contour, the functional in Eq. (32) can be properly modified as

$$\tilde{\Theta}(\boldsymbol{\xi}) = \sum_{i=1}^{N_\gamma} \int_{\Gamma_i} [w(x, y) - \tilde{w}_i(x, y)]^2 d\gamma \quad (46)$$

where $w(x, y)$ is given in Eq. (29) and $\tilde{w}_i(x, y)$ is an additional function, conveniently introduced to take into account the possibility of boundary deflections. Similarly to $\tilde{M}(x, y)$ in Eq. (37), $\tilde{w}_i(x, y)$ represents the pertinent deflection function evaluated on the boundary. Expressing $\tilde{w}_i(x, y)$ in terms of harmonic polynomials, yields

$$\tilde{w}_i(x, y) = \sum_{k=0}^{\tilde{m}} \tilde{c}_{k,i} P_k(x, y) + \sum_{k=1}^{\tilde{m}} \tilde{d}_{k,i} Q_k(x, y); \quad i = 1, \dots, N_\gamma \quad (47)$$

in which $\tilde{c}_{k,i}$ and $\tilde{d}_{k,i}$ are unknown coefficients to be determined, while \tilde{m} is the chosen truncation limit of the series expansion, with $\tilde{m} < m$ and generally small.

Denoting as

$$\mathbf{p}_{\tilde{m}}(x, y) = \begin{bmatrix} P_0(x, y) \\ \vdots \\ P_{\tilde{m}}(x, y) \end{bmatrix}; \quad \mathbf{q}_{\tilde{m}}(x, y) = \begin{bmatrix} Q_1(x, y) \\ \vdots \\ Q_{\tilde{m}}(x, y) \end{bmatrix}; \quad \tilde{\mathbf{c}}_i = \begin{bmatrix} \tilde{c}_{0,i} \\ \vdots \\ \tilde{c}_{\tilde{m},i} \end{bmatrix}; \quad \tilde{\mathbf{d}}_i = \begin{bmatrix} d_{1,i} \\ \vdots \\ \tilde{b}_{\tilde{m},i} \end{bmatrix} \quad (48)$$

Eq. (47) can conveniently be rewritten in compact form as

$$\tilde{w}_i(x, y) = \mathbf{s}_{\tilde{m}}^T \tilde{\boldsymbol{\xi}}_i; \quad i = 1, \dots, N_\gamma \quad (49)$$

where

$$\mathbf{s}_{\tilde{m}} = \begin{bmatrix} \mathbf{p}_{\tilde{m}}^T & \mathbf{q}_{\tilde{m}}^T \end{bmatrix}; \quad \tilde{\boldsymbol{\xi}}_i = \begin{bmatrix} \tilde{\mathbf{c}}_i \\ \tilde{\mathbf{d}}_i \end{bmatrix} \quad (50)$$

Further, taking into account Eqs. (30) and (49) and substituting in Eq. (46), yields the functional in the form

$$\tilde{\Theta}(\boldsymbol{\xi}) = \sum_{i=1}^{N_\gamma} \int_{\Gamma_i} \left[\mathbf{r}_m \boldsymbol{\xi} + w_p(x, y) - \mathbf{s}_{\tilde{m}}^T \tilde{\boldsymbol{\xi}}_i \right]^2 d\gamma \quad (51)$$

Note that, the additional function $\tilde{w}_i(x, y)$ in Eq. (46) must be taken into account only for the plate edges Γ_i which can undergo vertical deflections (such as for a free edge). Therefore, unless at least one edge is allowed to move vertically, $\tilde{w}_i(x, y) = 0 \forall i$, that is $\tilde{\boldsymbol{\xi}}_i = \mathbf{0}$, and the functional in Eq. (46) reverts to the more simple one in Eq. (32).

As far as the solution procedure is concerned, a three steps scheme, similar to the one described in Section 3.1, can be followed.

The first step is associated with the solution of Eq. (5.a), which leads to the moment sum function $M(x, y)$. In this regard, minimising the functional in Eq. (45), that is performing the variation of the functional with respect to the unknown coefficients $\boldsymbol{\eta}$, yields

$$\frac{\partial \tilde{\Psi}(\boldsymbol{\eta})}{\partial \boldsymbol{\eta}} = \mathbf{Q}_n \boldsymbol{\eta} + \boldsymbol{\tau} - \sum_{i=1}^{N_\gamma} \tilde{\mathbf{Q}}_{n,i} \tilde{\boldsymbol{\eta}}_i = \mathbf{0} \quad (52)$$

which is an algebraic linear system of equations, where

$$\tilde{\mathbf{Q}}_{n,i} = 2 \int_{\Gamma_i} \mathbf{r}_n^T \mathbf{s}_{\tilde{m}} d\gamma; \quad i = 1, \dots, N_\gamma \quad (53)$$

Equation (52) can equivalently be rewritten as

$$\boldsymbol{\eta} = -\mathbf{Q}_n^{-1} \boldsymbol{\tau} + \sum_{i=1}^{N_\gamma} \mathbf{Q}_n^{-1} \tilde{\mathbf{Q}}_{n,i} \tilde{\boldsymbol{\eta}}_i \quad (54)$$

so as to express the sought coefficients $\boldsymbol{\eta}$ in terms of the vectors $\tilde{\boldsymbol{\eta}}_i$.

Note that, as previously stated, if the plate BCs do not vary on the contour Γ , the functional in Eq. (37) should be used instead of the one in Eq. (45); thus, in this case, $N_\gamma = 1$ and the line integral in Eq. (53) simply reverts to a contour integral in Γ .

In this manner, considering Eq. (19) the moment sum function $M(x, y)$ can be directly expressed as

$$M(x, y) = -\mathbf{r}_n \mathbf{Q}_n^{-1} \boldsymbol{\tau} + \sum_{i=1}^{N_\gamma} \mathbf{r}_n \mathbf{Q}_n^{-1} \tilde{\mathbf{Q}}_{n,i} \tilde{\boldsymbol{\eta}}_i + M_p(x, y) \quad (55)$$

and a particular solution of Eq. (5.b) $w_p(x, y)$, which is required for the definition of the functional in Eq. (51), can be evaluated as reported in the Appendix A. It is worth stressing that, since $M(x, y)$ depends on $\tilde{\boldsymbol{\eta}}_i$ as shown in Eq. (55), also $w_p(x, y)$ will be a function of the unknown $\tilde{\boldsymbol{\eta}}_i$. To directly express this dependence, hereinafter the particular solution will be denoted as $w_p(x, y, \tilde{\boldsymbol{\eta}}_i)$.

The second step is associated with the solution of Eq. (5.b), which yields the deflection function $w(x, y)$. In this regard, the variation of the functional in Eq. (51), with respect to the unknown coefficients $\boldsymbol{\xi}$, can be performed as

$$\frac{\partial \tilde{\Psi}(\boldsymbol{\xi})}{\partial \boldsymbol{\xi}} = \mathbf{Q}_m \boldsymbol{\xi} + \boldsymbol{\lambda} - \sum_{i=1}^{N_\gamma} \tilde{\mathbf{Q}}_{m,i} \tilde{\boldsymbol{\xi}}_i = \mathbf{0} \quad (56)$$

where

$$\tilde{\mathbf{Q}}_{m,i} = 2 \int_{\Gamma_i} \mathbf{r}_m^T \mathbf{s}_{\tilde{m}} d\gamma; \quad i = 1, \dots, N_\gamma \quad (57)$$

whose solution leads to the coefficients $\boldsymbol{\xi}$ in terms of the unknowns $\tilde{\boldsymbol{\xi}}_i$, that is

$$\boldsymbol{\xi} = -\mathbf{Q}_m^{-1} \boldsymbol{\lambda} + \sum_{i=1}^{N_\gamma} \mathbf{Q}_m^{-1} \tilde{\mathbf{Q}}_{m,i} \tilde{\boldsymbol{\xi}}_i \quad (58)$$

Once these coefficients are found, the deflection function $w(x, y)$ can be evaluated substituting Eq. (58) into Eq. (30), as

$$w(x, y) = -\mathbf{r}_m \mathbf{Q}_m^{-1} \boldsymbol{\lambda} + \sum_{i=1}^{N_\gamma} \mathbf{r}_m \mathbf{Q}_m^{-1} \tilde{\mathbf{Q}}_{m,i} \tilde{\boldsymbol{\xi}}_i + w_p(x, y, \tilde{\boldsymbol{\eta}}_i) \quad (59)$$

Finally, the unknown terms $\tilde{\eta}_i$ and $\tilde{\xi}_i$ can be obtained appropriately imposing the specified BCs on the edges Γ_i for which the additional functions $\tilde{M}_i(x, y)$ and $\tilde{w}_i(x, y)$ have been introduced. Specifically, for the most common cases, taking into account Eqs. (6, 9, 10) the following functionals can be defined for each edge Γ_i of the whole plate contour Γ :

i. Simply-supported curved edge

$$\Xi_i(\tilde{\eta}_i) = \int_{\Gamma_i} [M_n(x, y)]^2 d\gamma \quad (60)$$

ii. Clamped edge

$$\Xi_i(\tilde{\eta}_i) = \int_{\Gamma_i} \left[\frac{\partial w(x, y)}{\partial n} \right]^2 d\gamma \quad (61)$$

iii. Free edge

$$\Xi_i(\tilde{\eta}_i) = \int_{\Gamma_i} [M_n(x, y)]^2 d\gamma \quad (62.a)$$

$$\Lambda_i(\tilde{\xi}_i) = \int_{\Gamma_i} [\tilde{V}_n(x, y)]^2 d\gamma \quad (62.b)$$

Note that, taking advantage of the properties of the harmonic polynomials, and considering the general expression of the deflection function in Eq. (59), all the aforementioned BCs in Eqs. (60)-(62) can be appropriately represented in compact matrix form. In this regard, for simplicity sake, the resulting expressions are reported in Appendix B.

In this context, observe that even more complex BCs, such as guided-end conditions, elastically restrained edges or imposed deflections, can be taken into account in a similar manner. Further, variations of the BCs on the same edge Γ_i can be considered as well, appropriately subdividing the pertinent edge Γ_i in the corresponding part on which the BCs remain constant.

Clearly, minimising the above defined functionals, that is performing the variation with respect to the unknown coefficients $\tilde{\eta}_i$ and $\tilde{\xi}_i$ as

$$\frac{\partial \Xi_i(\tilde{\eta}_i)}{\partial \tilde{\eta}_i} = \mathbf{0} \quad (63.a)$$

$$\frac{\partial \Lambda_i(\tilde{\xi}_i)}{\partial \tilde{\xi}_i} = \mathbf{0} \quad (63.b)$$

yields an algebraic linear system of equations in terms of $\tilde{\eta}_i$ and $\tilde{\xi}_i$, which can be easily solved for the sought coefficients. Further substitution in Eq. (59) leads to the complete definition of deflection function $w(x, y)$.

To further elucidate the mechanics of the technique, Fig. 3 provides a step-by-step flowchart for the method, where reference to the aforementioned steps is reported as well.

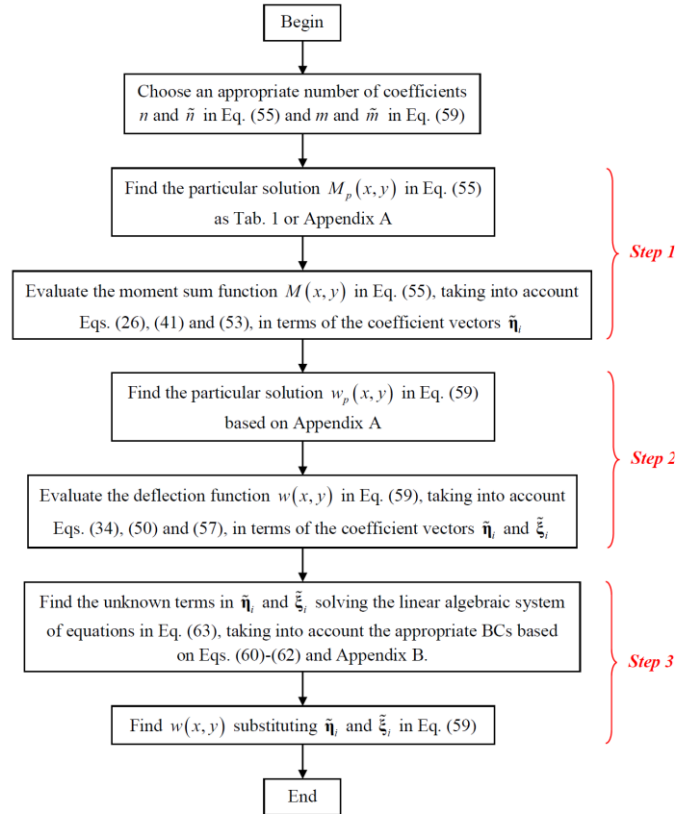


Fig. 3 Flowchart of the method

It is worth noting that the entire procedure only requires the definition of simple line integrals, and the solution of algebraic linear system of equations which can be performed in a straightforward manner in any symbolic computation programs, such as Wolfram Mathematica.

On this base, a peculiar characteristic of the proposed approach for plate analysis is the possibility of recovering the exact closed-form solution of the problem when it exists, as it will be shown in the following section, while in the other cases the method yields an approximate analytical solution, and this may be regarded as an attractive feature of the proposed procedure with respect to classical FEM and meshless approaches, which can provide only numerical results.

Notably, the method does not require the definition of any mesh, and few terms in the series expansions are generally needed, thus keeping at minimum the computational effort. Finally, since

neither the domain nor the boundary must be discretized (as in the classical FEM or BEM), the same procedure and expressions can be applied for different plate geometries, once the contour of the plate has been appropriately parameterized.

4 Applications

In this section, the proposed LEM approach is applied to several plate configurations, considering various shapes, boundary conditions and both distributed and concentrated loads. Firstly, as benchmark cases, the proposed method is employed for three different well-known examples, namely triangular simply-supported plate, circular clamped plate and elliptical clamped plate, demonstrating the ability of the method to directly yield the exact solutions. Further, as approximate analytical solutions, a rectangular shaped plate with mixed boundary conditions, a triangular simply-supported plate under a concentrated load and a plate with complex shape are investigated to show the potentiality of the method. Finally, to assess the accuracy of the procedure, the LEM based deflection functions are compared with the results of classical Finite Element analyses for all the above mentioned configurations, providing also relative errors data are also.

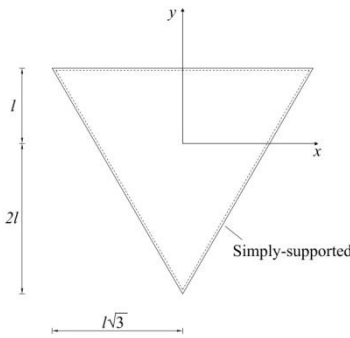
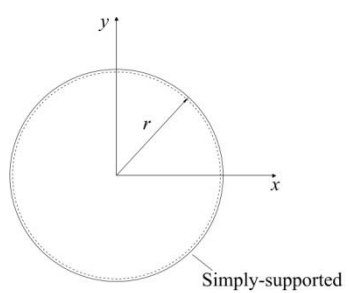
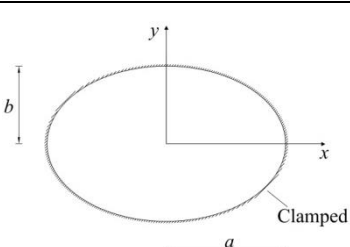
As far as the selection of the number of terms in Eqs. (17), (29), (38) and (47) is concerned for these numerical applications, it is noted that these values strongly depend on the specific problem under consideration. In this regard, in general, greater values might be required for determining the deflection of plates with complex shapes or BCs, and in case of complex load functions. Further, an higher number of terms is generally necessary if stress distributions on the boundaries are sought. Obviously, higher number of terms leads to enhanced accuracy, at the expense, however, of higher computational cost. Readers may refer to the following numerical examples for potential candidate values of the parameters. Further, as a rule of thumb for choosing an appropriate number of terms, the procedure in Fig. 3 can be performed for few different values of n and m , since the approach generally requires few seconds in terms of computational cost. For increasing values of these parameters, a good indication that the specific value is a reasonable one is when no considerable difference is noted anymore in the form of the plate deflection, and the BCs are appropriately satisfied, as shown in the following section.

4.1 Numerical applications: exact solutions

Consider the case of a triangular shaped plate (see Tab. 2) under a uniformly distributed load $q(x, y) = q_0$ and with all the edges simply-supported. Applying the previously described procedure

yields the non-null series coefficients for the deflection function Eq. (30) of the vector ξ , as reported in Tab. 2.

Tab. 2: Plate geometries and corresponding coefficients of the deflection function.

| Plate Shape and BCs | Non-null coefficients of $w(x, y)$ |
|--|---|
|  <p style="text-align: center;">Simply-supported</p> | $c_0 = \frac{q_0 l^4}{12D}; \quad c_2 = \frac{q_0 l^2}{12D}; \quad c_4 = \frac{q_0}{64D};$ $d_3 = \frac{q_0 l}{48D}; \quad d_5 = \frac{q_0}{192lD};$ |
|  <p style="text-align: center;">Simply-supported</p> | $c_0 = \frac{q_0 r^4 (5+\nu)}{64D(1+\nu)}; \quad c_2 = \frac{q_0 r^2 (3+\nu)}{32D(1+\nu)}; \quad c_4 = \frac{q_0}{64D}$ |
|  <p style="text-align: center;">Clamped</p> | $c_0 = \frac{q_0 a^4 b^4}{8\beta D}; \quad c_2 = \frac{q_0 a^2 b^2}{4\beta D}; \quad c_4 = \frac{q_0 a^4}{8\beta D}$ $\beta = (3a^4 + 2a^2 b^2 + 3b^4)$ |

Substituting in Eq. (30) leads to

$$w(x, y) = \left(\frac{q_0}{192lD} \right) \left[-y^3 + 3x^2y - 3l(x^2 + y^2) + 4l^3 \right] (l^2 - x^2 - y^2) \quad (64)$$

which is the exact solution of the considered problem [1]. In this regard, the contours of the above obtained deflection function are shown in Fig. 4(a) for $l = \sqrt{3}/6 \text{ m}$.

Consider next the case of a circular plate (see Tab. 2) of radius r under a uniformly distributed load q_0 and simply-supported along the entire contour ($N_\gamma = 1$). The plate boundary Γ is defined by the curve in parametric form

$$\begin{cases} x = r \cos \theta \\ y = r \sin \theta \end{cases}, \quad 0 \leq \theta \leq 2\pi \quad (65)$$

Since the boundary is curvilinear, the additional moment sum function $\tilde{M}_1(x, y)$ should be taken into account, while $\tilde{w}_1(x, y)$ is equal to zero, that is $\tilde{\xi}_1 = 0$, because of the chosen BCs. Applying the previously defined procedure, coefficients η and ξ are found via Eq. (54) and (58), respectively, in terms of the unknowns $\tilde{\eta}_1$. Finally, considering Eq. (59), the remaining coefficients \tilde{a}_k and \tilde{b}_k in $\tilde{\eta}_1$ are found using Eq. (60). In this regard, a value of $\tilde{a}_0 = -\frac{q_0 r^2 (\nu - 1)}{8(1 + \nu)}$ is obtained, while all the other terms are equal to zero. Therefore, substituting in Eq. (59) yields the well-known exact solution of the deflection function as

$$w(x, y) = \frac{q_0 (r^2 - x^2 - y^2) \left[-(x^2 + y^2)(1 + \nu) + r^2(5 + \nu) \right]}{64 D (1 + \nu)} \quad (66)$$

In this regard, the contours of the function in Eq. (66) are shown in Fig. 4(b) for $r = 1m$.

Finally, consider the case of a clamped elliptical plate of axes a and b (see Tab. 2), under a uniformly distributed load q_0 . The plate boundary Γ is defined by the curve in parametric form

$$\begin{cases} x = a \cos \theta \\ y = b \sin \theta \end{cases}, \quad 0 \leq \theta \leq 2\pi \quad (67)$$

As in the previous case, taking into account the BCs and the plate shape, $N_\gamma = 1$, $\tilde{M}_1(x, y) \neq 0$ and $\tilde{w}_1(x, y) = 0$. Following the previously described procedure, all the pertinent coefficients are found minimizing the functional in Eq. (60) considering Eqs. (54) and (58), leading to the deflection function

$$w(x, y) = \frac{q_0 \left[b^2 x^2 + a^2 (-b^2 + y^2) \right]^2}{8(3a^4 + 2a^2 b^2 + 3b^4) D} \quad (68)$$

which is the exact solution of the problem [1]. In this regard, the contours of Eq. (68) are shown in Fig. 4(c) for $a = 1.5m$ and $b = 1m$.

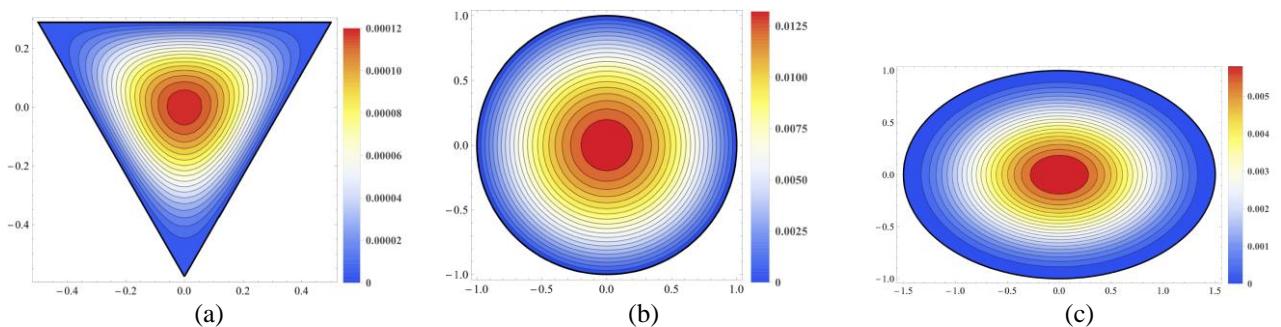


Fig. 4 Deflection functions $w(x, y)$ for $q_0 = 500 \text{ N/m}^2$; $h = 5 \text{ mm}$; $E = 210 \text{ GPa}$; $\nu = 0.3$: (a) Triangular simply-supported plate; (b) Circular simply-supported plate; (c) Elliptical clamped plate.

As far as the convergence rates of the proposed approach is concerned, analyses can be performed in terms of the L_2 displacement and energy norm, which can be defined respectively as [18]

$$\|w\| = \left[\int_{\Omega} w(x, y)^2 d\Omega \right]^{\frac{1}{2}} \quad (69)$$

and

$$\|e\| = \frac{D}{2} \left[\int_{\Omega} \nabla^2 w(x, y)^2 d\Omega \right]^{\frac{1}{2}} \quad (70)$$

In Tab. 3 the relative error between the L_2 displacement and energy norm of the exact solution and the proposed approach, for different values of the number of coefficients m in Eq. (29) is reported. As it can be seen, relative error is exactly equals to zero for the highest number of terms in the series expansion since, as previously mentioned, the proposed method leads to the analytical solutions.

Tab. 3. Relative errors in terms of L_2 displacement and energy norm

| <i>Plate Shape and BCs</i> | <i>Number of coefficients m</i> | <i>Relative error for the L_2 displacement norm</i> | <i>Relative error for the L_2 energy norm</i> |
|--|--|--|--|
| <i>Triangular simply-supported plate</i> | $m = 5$ | 0 | 0 |
| | $m = 4$ | $3.42 \cdot 10^{-2}$ | $3.33 \cdot 10^{-1}$ |
| | $m = 3$ | $1.27 \cdot 10^{-1}$ | $7.11 \cdot 10^{-1}$ |
| <i>Circular simply-supported plate</i> | $m = 4$ | 0 | 0 |
| | $m = 3$ | $4.93 \cdot 10^{-3}$ | $5.37 \cdot 10^{-3}$ |
| | $m = 2$ | $4.93 \cdot 10^{-3}$ | $5.37 \cdot 10^{-3}$ |
| <i>Elliptical clamped plate</i> | $m = 4$ | 0 | 0 |
| | $m = 3$ | 1.89 | 1.13 |
| | $m = 2$ | 1.89 | 1.13 |

Further details on the convergence of the method can be obtained graphically, plotting for instance the deflection functions of the plate boundaries which, for the considered cases, must be null. In this regard, in Fig. 5 deflection functions on the boundaries are shown for the same number of coefficients m used in Tab. 3. Specifically, in Fig. 5(a) the plate deflection on the horizontal edge of the triangular plate is shown, while in Figs. 5(b) and (c) the circumferential deflections of the circular and elliptical plate boundaries are reported.

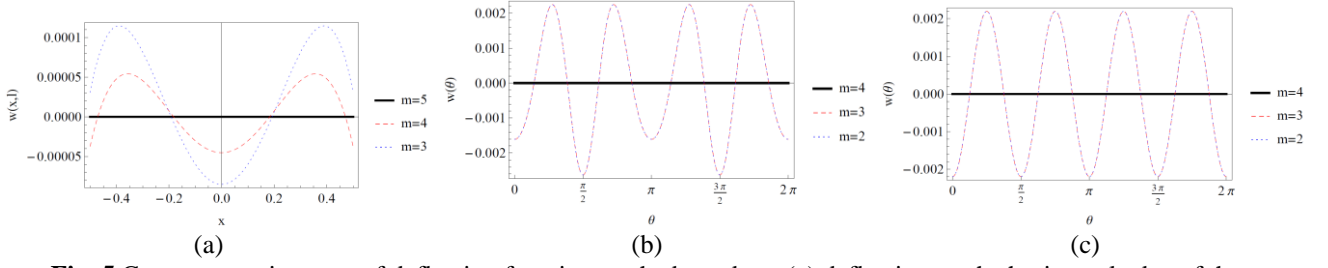


Fig. 5 Convergence in terms of deflection function on the boundary: (a) deflection on the horizontal edge of the triangular plate; (b) circumferential deflection of the circular plate; (c) circumferential deflection of the elliptical plate.

Note that, deflections exactly equal to zero for the highest number of terms continuously on the whole contour, since the analytical solutions are reached. Further, as shown in Fig. 5(b) and (c), deflections obtained with $m = 3$ exactly match those obtained using $m = 2$ since, as reported in Tab. 2, coefficients c_3 and d_3 are equal to zero.

Note that, classically to obtain the above reported exact solutions in Eqs. (64), (66) and (68) different approaches are required for each plate shape [1]. For instance, solution of circular and elliptical plates is generally obtained considering polar and elliptical coordinates. On the other hand, as shown, the proposed method yields the exact solutions, if available, regardless the chosen plate geometry.

In the following section, LEM will be applied to different plate configurations, aiming at highlighting the ability of the proposed approach to treat more demanding cases, such as generic load conditions, mixed BCs and plate of complex shape.

4.2 Numerical application: concentrated load

As a first example, in order to show how the proposed procedure can also be applied for plate under generic load conditions, consider the case of a simply-supported triangular plate under a concentrated load \bar{Q} applied at the origin.

Since in this case \bar{Q} cannot be directly expressed as in Eq. (21), the concentrated load can be assumed as a distributed load $q(x, y)$ shaped as a Dirac's delta $\delta(x, y)$ of amplitude equals to \bar{Q} , which can be conveniently approximated in terms of Chebyshev polynomials as

$$q(x, y) \approx \bar{Q} \left(\frac{1}{\pi} T_0(x) + \frac{2}{\pi} \sum_{s=1}^N (-1)^s T_{2s}(x) \right) \left(\frac{1}{\pi} T_0(y) + \frac{2}{\pi} \sum_{s=1}^N (-1)^s T_{2s}(y) \right) \quad (71)$$

where N is the truncation limit of the series expansion, while $T_s(\cdot)$ is the Chebyshev polynomial of order s , defined by the recurrence relation [43]

$$T_{s+1}(x) = 2xT_s(x) - T_{s-1}(x) \quad (72)$$

in which $T_0(x) = 1$ and $T_1(x) = x$.

Once the concentrated load has been expressed as in Eq. (71), the particular solution $M_p(x, y)$ of Eq. (5.a) can be obtained in closed-form using the approach in Appendix A.

In this manner, the above defined procedure can be easily applied. Specifically, taking into account the chosen plate shape and BCs, the procedure in section 3.1 can be followed. Thus, firstly the moment sum function $M(x, y)$ is directly determined via Eq. (28) and secondly the deflection function $w(x, y)$ is immediately retrieved using Eq. (36).

In this regard, Fig. 6(a) shows the contour plot of the aforementioned function, assuming $l = \sqrt{3}/6m$. Note that in this case 22 terms have been used in the vector ξ in Eq.(35), considering only even coefficients c_{2k} and odd coefficients d_{2k+1} (thus also $m = 22$ in Eq. 29). Further, in Fig. 6(b) LEM results of the deflection profile at $x = 0$ are compared with pertinent FEM data obtained employing the commercial code Ansys.

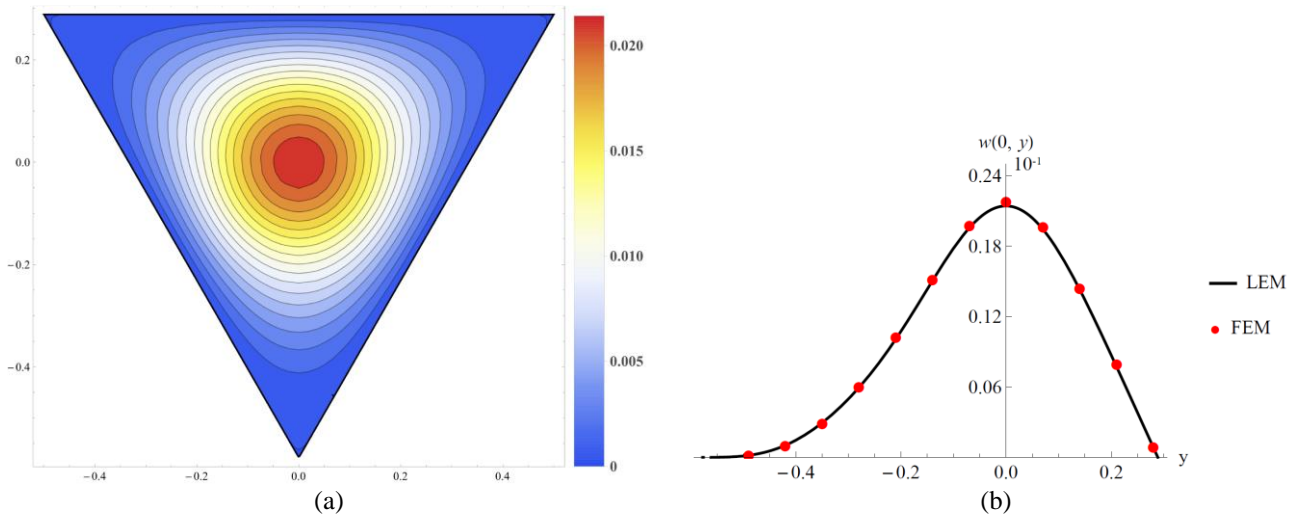


Fig. 6 Deflection functions $w(x, y)$ for $\bar{Q} = 100 N$; $h = 1 \text{ mm}$; $E = 210 \text{ GPa}$; $\nu = 0.3$: (a) Contours plot with LEM; (b) Deflection profile.

As it can be observed, classical FEM data are in very good agreement with the results of the proposed LEM approach, assessing the accuracy of the considered procedure.

To further assess the reliability of the procedure, the average relative discrepancy index $\bar{\varepsilon}_r$ between proposed method results and FEM data has been computed. Specifically, $\bar{\varepsilon}_r$ can be defined as

$$\bar{\varepsilon}_r = \frac{1}{N_p} \sqrt{\frac{(w_{LEM} - w_{FEM})^2}{w_{FEM}^2}} \cdot 100 \quad (73)$$

where w_{LEM} and w_{FEM} are the values of the deflection obtained using the LEM and FEM approach respectively, while N_p is the considered number of points of the deflection functions.

In this regard, taking into account the points in Fig. 6(b), $\bar{\varepsilon}_r = 1.75\%$, thus showing the accuracy of the propose approach.

4.3 Numerical application: mixed BCs

Aiming at demonstrating the capability of the proposed procedure to treat plates with mixed BCs., consider the case of a rectangular plate under a uniformly distributed load q_0 , assuming two opposite plate edges simply-supported, one edge clamped and one free, as shown in Fig. 7(a).

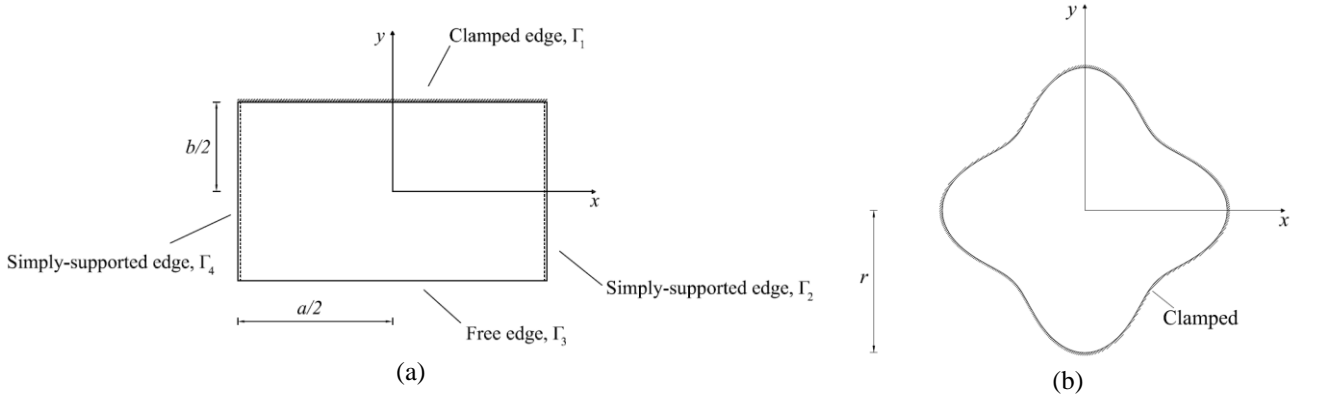


Fig. 7 Plate geometries: (a) Rectangular plate with mixed BCs; (b) Clamped plate of complex shape.

Applying the procedure in Section 3.2, the plate boundary Γ can be conveniently subdivided in four edges Γ_i , that is $N_\gamma = 4$. Note that, since the two edges Γ_2 and Γ_4 are simply-supported, as previously mentioned the corresponding function $\tilde{M}_2(x, y)$ and $\tilde{M}_4(x, y)$ in Eq. (42) can be assumed equal to zero and only the remaining functions $\tilde{M}_1(x, y)$ and $\tilde{M}_3(x, y)$ must be taken into account. Further, since just the boundary Γ_3 can undergo vertical deflections, $\tilde{w}_3(x, y) \neq 0$ while $\tilde{w}_i(x, y) = 0, i = 1, 2, 3$ in Eq. (46).

In this manner, the vector $\boldsymbol{\eta}$ in Eq. (54) can be specified as

$$\boldsymbol{\eta} = -\mathbf{Q}_n^{-1} \boldsymbol{\tau} + \mathbf{Q}_n^{-1} \tilde{\mathbf{Q}}_{n,1} \tilde{\boldsymbol{\eta}}_1 + \mathbf{Q}_n^{-1} \tilde{\mathbf{Q}}_{n,3} \tilde{\boldsymbol{\eta}}_3 \quad (74)$$

and the moment sum function $M(x, y)$ can be obtained via Eq. (20).

Further, the vector $\boldsymbol{\xi}$ in Eq. (58) becomes

$$\boldsymbol{\xi} = -\mathbf{Q}_m^{-1} \boldsymbol{\lambda} + \mathbf{Q}_m^{-1} \tilde{\mathbf{Q}}_{m,3} \tilde{\boldsymbol{\xi}}_3 \quad (75)$$

and the deflection function can be evaluated substituting in Eq. (30) as

$$w(x, y) = -\mathbf{r}_m \mathbf{Q}_m^{-1} \boldsymbol{\lambda} + \mathbf{r}_m \mathbf{Q}_m^{-1} \tilde{\mathbf{Q}}_{m,3} \tilde{\boldsymbol{\xi}}_3 + w_p(x, y, \tilde{\boldsymbol{\eta}}_1, \tilde{\boldsymbol{\eta}}_3) \quad (76)$$

Finally, the unknown terms $\tilde{\boldsymbol{\eta}}_1$, $\tilde{\boldsymbol{\eta}}_3$ and $\tilde{\boldsymbol{\xi}}_3$ can be obtained appropriately imposing the specified BCs on the edges Γ_1 and Γ_3 for which the additional functions $\tilde{M}_i(x, y)$ and $\tilde{w}_i(x, y)$ have been introduced.

Specifically, minimizing the functional in Eq. (62) specified for Γ_3 , namely $\Xi_3(\tilde{\boldsymbol{\eta}}_3)$ and $\Lambda_3(\tilde{\boldsymbol{\xi}}_3)$, as in Eq. (63), the vectors $\tilde{\boldsymbol{\eta}}_3$ and $\tilde{\boldsymbol{\xi}}_3$ can be obtained in terms of $\tilde{\boldsymbol{\eta}}_1$. Finally, minimization of the functional in Eq. (61) for Γ_1 , that is $\Xi_1(\tilde{\boldsymbol{\eta}}_1)$, yields the vector $\tilde{\boldsymbol{\eta}}_1$. Clearly, further substitution in Eq. (76) leads to the complete definition of deflection function $w(x, y)$.

In this regard in Fig. 8(a) the contour plot of the deflection function is shown, assuming $a = 1\text{ m}$ and $b = 0.5\text{ m}$. Note that in this case 12 coefficients c_k and 10 coefficients d_k have been used in the vector $\boldsymbol{\xi}$. Further, proposed method results vis-à-vis FEM data are shown in Fig. 8(b) for the deflection profile at $x = 0$.

As it can be seen, an excellent agreement is achieved between classical FEM data and proposed LEM approach, assessing the accuracy of the considered procedure.

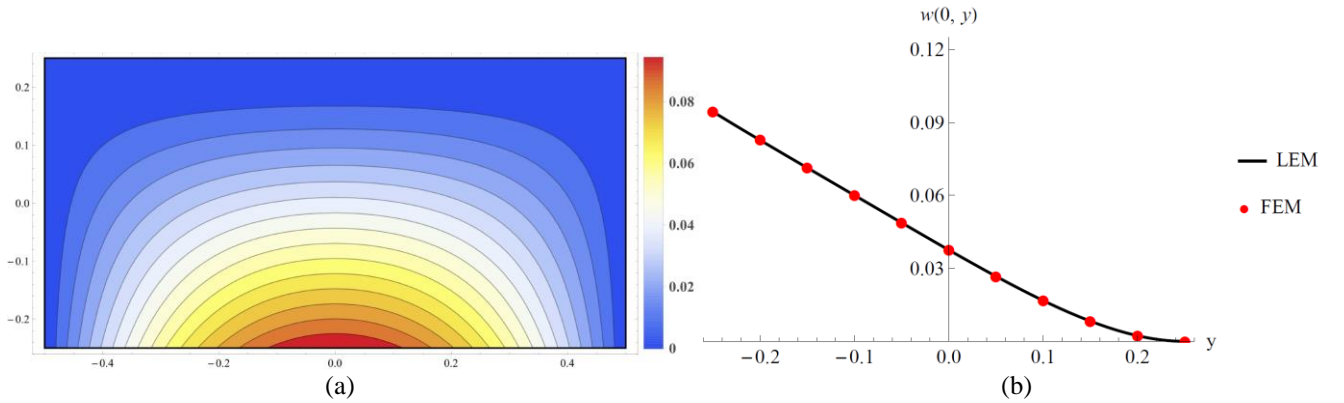


Fig. 8 Deflection functions $w(x, y)$ for $q_0 = 500\text{ N/m}^2$; $h = 1\text{ mm}$; $E = 210\text{ GPa}$; $\nu = 0.3$: (a) Contours plot with LEM; (b) Deflection profile.

To further show the reliability of the approach, the average relative discrepancy index in Eq. (73) has been computed, considering the points in Fig. 8(b), leading to the very low value of $\bar{\varepsilon}_r = 0.28\%$

4.4 Numerical application: arbitrarily shaped plate

As a final example, to demonstrate the capability of the method to treat plates with arbitrary geometries, a clamped plate with complex shape (see Fig. 7(b)) under uniformly distributed load q_0 has been analyzed. The boundary Γ of the plate is defined by the curve in parametric form

$$\begin{cases} x = r \left(|\sin \theta|^3 + |\cos \theta|^3 \right) \cos \theta \\ y = r \left(|\sin \theta|^3 + |\cos \theta|^3 \right) \sin \theta \end{cases}, \quad 0 \leq \theta \leq 2\pi \quad (77)$$

Applying the proposed procedure, considering the specified BCs, the moment sum function can be expressed as

$$M(x, y) = -\mathbf{r}_n \mathbf{Q}_n^{-1} \boldsymbol{\tau} + \mathbf{r}_n \mathbf{Q}_n^{-1} \tilde{\mathbf{Q}}_{n,1} \tilde{\boldsymbol{\eta}}_1 + M_p(x, y) \quad (78)$$

where $\tilde{\boldsymbol{\eta}}_1$ is a vector of unknowns due to the additional function $\tilde{M}_1(x, y)$ which takes into account the clamped BCs, while $M_p(x, y)$ is given in Tab. 1 for the uniform load distribution.

Further, since no deflection occurs on Γ , $\tilde{\xi}_i = 0$ and the deflection function in Eq. (59) can be simplified as

$$w(x, y) = -\mathbf{r}_m \mathbf{Q}_m^{-1} \boldsymbol{\lambda} + w_p(x, y, \tilde{\boldsymbol{\eta}}_1) \quad (79)$$

where the particular solution $w_p(x, y, \tilde{\boldsymbol{\eta}}_1)$ can be obtained as in Appendix A.

Finally, the unknown term $\tilde{\boldsymbol{\eta}}_1$ can be evaluated appropriately imposing the specified BCs on Γ . Specifically, performing variation of the functional in Eq. (61) with respect to $\tilde{\boldsymbol{\eta}}_1$ yields a linear system of algebraic equation, whose solution leads to the unknowns coefficients $\tilde{\boldsymbol{\eta}}_1$.

In this regard, the contours of the deflected surface for $r = 1m$ is depicted in Fig. 9(a), while in Fig. 9(b) the deflection profile at $x = 0$ is reported vis-à-vis pertinent FEM data. Note that, in this case just 9 terms of the even coefficients c_{2k} are required in the vector $\boldsymbol{\xi}$ in Eq. (58) (that is $m = 16$), being zero all the coefficients c_{2k+1} and d_k .

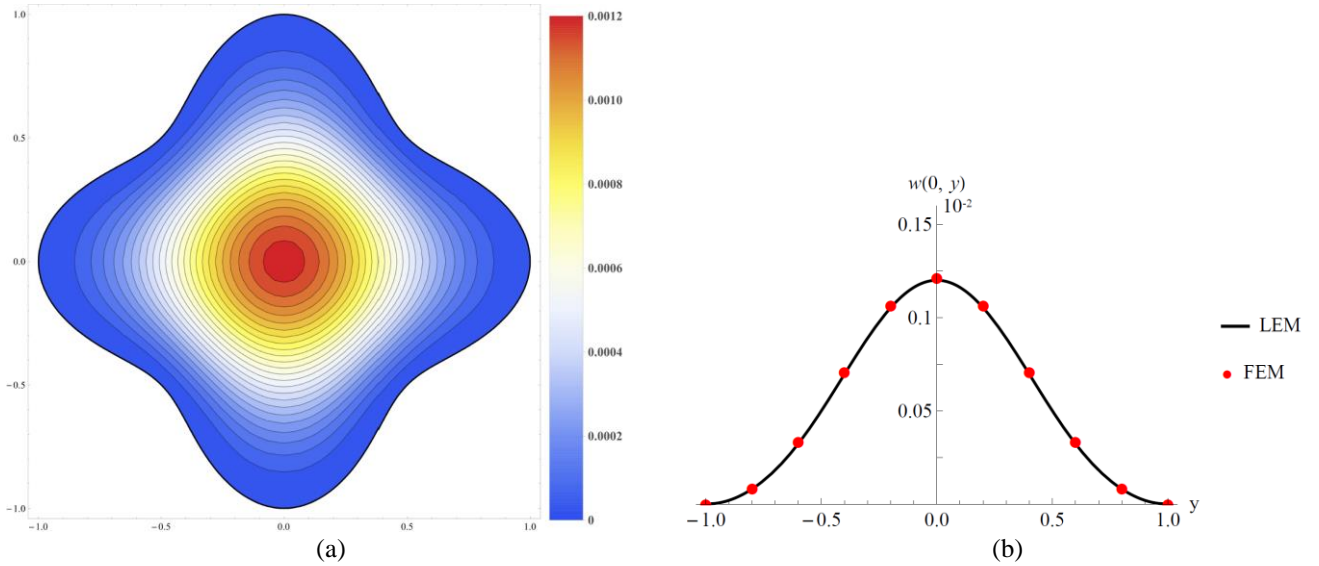


Fig 9 Deflection functions $w(x, y)$ for $q_0 = 500 \text{ N/m}^2$; $h = 5 \text{ mm}$; $E = 210 \text{ GPa}$; $\nu = 0.3$: (a) Contours plot with LEM; (b) Deflection profile.

As it can be observed, also in this case an excellent agreement is achieved between proposed and FEM data, further assessing the reliability of the proposed procedure. Moreover, the average relative discrepancy index in Eq. (73) has been computed, considering the points in Fig.9(b), leading to the satisfactorily low value $\bar{\varepsilon}_r = 1.83\%$

Concluding Remarks

In this paper, an innovative procedure has been developed for evaluating the deflection function of arbitrarily shaped plates subject to generic transverse loading conditions. This approach, which can be framed into the Line Element-less Method (LEM), allows to evaluate the plate deflection function through a simple series expansion in terms of harmonic polynomials. Appropriately defining novel functionals and performing variations, linear systems of algebraic equations have been obtained for the series expansion coefficients. Further, considered boundary conditions have been satisfied via an element-free procedure in a least square sense on the plate contour. Notably, only simple line integrals are involved in the whole procedure, and any discretization, be it in the domain or on the boundary, has been avoided. Additionally, it has been shown that the method leads to exact solutions, when available, for different plates geometries and boundary conditions, while for all the other cases highly accurate approximate analytical results have been achieved using few terms in the series expansions. Analyses have been carried out for several plate shapes, boundary and loading conditions, showing the elegance and simplicity of the proposed procedure, which allows the computational cost to be kept at minimum. Further, for all these cases,

comparisons of LEM based deflection functions vis-à-vis pertinent Finite Element method data have been reported, assessing the accuracy and reliability of the considered approach.

Acknowledgement

Alberto Di Matteo and Antonina Pirrotta would like to acknowledge the PRIN 2015 funding program from the Italian Ministry of University and Research (MIUR), Project N. 2015JW9NJT.

Appendix A: Particular solution for Poisson's equation

In this appendix, the procedure described in [41] to obtain a closed form expression of a particular solution of a Poisson's equation is briefly reported.

In this regard, consider a Poisson's equation of the form

$$\nabla^2 f(x, y) = q(x, y) \quad (\text{A.1})$$

where $q(x, y)$ is a generic homogeneous polynomial of degree N given as

$$q(x, y) = \sum_{k=0}^N A_k x^{N-k} y^k \quad (\text{A.2})$$

Then, a closed form particular solution of Eq. (A.1) is

$$f_p(x, y) = \sum_{k=0}^N \tilde{P}_k x^{N-k+2} y^k \quad (\text{A.3})$$

that is a polynomial of degree N , where the coefficients \tilde{P}_k are

$$\tilde{P}_k = \sum_{m=0}^{\lfloor (N-k)/2 \rfloor} \frac{(-1)^m (k+2m)! (N-k-2m)!}{k! (N-k+2)!} A_{k+2m}; \quad 1 \leq k \leq N \quad (\text{A.4})$$

Note that, in Eq. (A.4) the term $\lfloor (N-k)/2 \rfloor$ denotes the integer part of $(N-k)/2$.

It is worth mentioning that, when $q(x, y)$ is not directly given as in Eq. (A.2), the particular solution in Eq. (A.3) can still be used if $q(x, y)$ is firstly appropriately approximated by a truncated series of Chebyshev polynomials [42, 43].

Appendix B: Expression of the Boundary Conditions in terms of Harmonic Polynomials

In this appendix, the compact form expressions of the BCs used in Eqs. (60)-(62) are reported. Specifically, taking into account Eq. (59) and the properties of the harmonic polynomials in Eqs. (15) and (16), it is possible to directly give explicit expressions of the BCs in terms of the previously introduced functions. In this regard, let the deflection function in Eq. (59) be rewritten as

$$w(x, y) = \mathbf{r}_m \boldsymbol{\mu} + w_p(x, y, \tilde{\eta}_i) \quad (\text{B.1})$$

where \mathbf{r}_m is a row vector containing the harmonic polynomials, as given in Eq. (31), while $\boldsymbol{\mu}$ is a column vector of coefficients, given as

$$\boldsymbol{\mu} = -\mathbf{Q}_m^{-1} \boldsymbol{\lambda} + \sum_{i=1}^{N_y} \mathbf{Q}_m^{-1} \tilde{\mathbf{Q}}_{m,i} \tilde{\boldsymbol{\xi}}_i \quad (\text{B.2})$$

In this manner, omitting henceforth variable dependence, derivatives of the deflection function can be expressed as

$$\frac{\partial w}{\partial x} = \frac{\partial \mathbf{r}_m}{\partial x} \boldsymbol{\mu} + \frac{\partial w_p}{\partial x} \quad (\text{B.3})$$

and

$$\frac{\partial w}{\partial y} = \frac{\partial \mathbf{r}_m}{\partial y} \boldsymbol{\mu} + \frac{\partial w_p}{\partial y} \quad (\text{B.4})$$

Recalling the properties of the harmonic polynomials as in Eq. (16), Eqs. (B.3) and (B.4) can be directly expressed in compact form as

$$\frac{\partial w}{\partial x} = \mathbf{r}_{m,x}^{(1)} \mathbf{Z}_x^{(1)} \boldsymbol{\mu} + \frac{\partial w_p}{\partial x} \quad (\text{B.5})$$

and

$$\frac{\partial w}{\partial y} = \mathbf{r}_{m,y}^{(1)} \mathbf{Z}_y^{(1)} \boldsymbol{\mu} + \frac{\partial w_p}{\partial y} \quad (\text{B.6})$$

where $\mathbf{Z}_x^{(1)}$ and $\mathbf{Z}_y^{(1)}$ are diagonal matrices of coefficients given respectively as $\mathbf{Z}_x^{(1)} = [\bar{0} \ 1 \cdots m \ 1 \ 2 \cdots \underline{m}]$ and $\mathbf{Z}_y^{(1)} = [\bar{0} \ 1 \cdots (-m) \ 1 \ 2 \cdots \underline{m}]$, while $\mathbf{r}_{m,x}^{(1)}$ and $\mathbf{r}_{m,y}^{(1)}$ are vectors containing the corresponding derivatives of \mathbf{r}_m , given as

$$\mathbf{r}_{m,x}^{(1)} = [P_{-1} \cdots P_{m-1} \ Q_0 \cdots Q_{m-1}] \quad (\text{B.7})$$

and

$$\mathbf{r}_{m,y}^{(1)} = [Q_{-1} \cdots Q_{m-1} \ P_0 \cdots P_{m-1}] \quad (\text{B.8})$$

On this base, second order derivatives can be directly obtained as

$$\frac{\partial^2 w}{\partial x^2} = \mathbf{r}_{m,x}^{(2)} \mathbf{Z}_x^{(1)} \mathbf{Z}_x^{(2)} \boldsymbol{\mu} + \frac{\partial^2 w_p}{\partial x^2} \quad (\text{B.9})$$

$$\frac{\partial^2 w}{\partial y^2} = \mathbf{r}_{m,y}^{(2)} \mathbf{Z}_y^{(1)} \mathbf{Z}_y^{(2)} \boldsymbol{\mu} + \frac{\partial^2 w_p}{\partial y^2} \quad (\text{B.10})$$

$$\frac{\partial^2 w}{\partial x \partial y} = \mathbf{r}_{m,xy}^{(2)} \mathbf{Z}_y^{(1)} \mathbf{Z}_x^{(2)} \boldsymbol{\mu} + \frac{\partial^2 w_p}{\partial x \partial y} \quad (\text{B.11})$$

where $\mathbf{Z}_x^{(2)} = \begin{bmatrix} -1 & 0 \cdots (m-1) & 0 & 1 \cdots (m-1) \end{bmatrix}$ and $\mathbf{Z}_y^{(2)} = \begin{bmatrix} -1 & 0 \cdots (m-1) & 0 & -1 \cdots -(m-1) \end{bmatrix}$,

while

$$\mathbf{r}_{m,x}^{(2)} = [P_{-2} \cdots P_{m-2} \ Q_{-1} \cdots Q_{m-2}] \quad (\text{B.12})$$

$$\mathbf{r}_{m,xy}^{(2)} = [Q_{-2} \cdots Q_{m-2} \ P_{-1} \cdots P_{m-2}] \quad (\text{B.13})$$

and $\mathbf{r}_{m,y}^{(2)} = \mathbf{r}_{m,x}^{(2)}$.

Finally, third order derivatives can be rewritten as

$$\frac{\partial^3 w}{\partial x^3} = \mathbf{r}_{m,x}^{(3)} \mathbf{Z}_x^{(1)} \mathbf{Z}_x^{(2)} \mathbf{Z}_x^{(3)} \boldsymbol{\mu} + \frac{\partial^3 w_p}{\partial x^3} \quad (\text{B.14})$$

$$\frac{\partial^3 w}{\partial y^3} = \mathbf{r}_{m,y}^{(3)} \mathbf{Z}_y^{(1)} \mathbf{Z}_y^{(2)} \mathbf{Z}_y^{(3)} \boldsymbol{\mu} + \frac{\partial^3 w_p}{\partial y^3} \quad (\text{B.15})$$

$$\frac{\partial^3 w}{\partial x \partial y^2} = \mathbf{r}_{m,xy}^{(3)} \mathbf{Z}_x^{(1)} \mathbf{Z}_y^{(2)} \mathbf{Z}_y^{(3)} \boldsymbol{\mu} + \frac{\partial^3 w_p}{\partial x \partial y^2} \quad (\text{B.16})$$

$$\frac{\partial^3 w}{\partial y \partial x^2} = \mathbf{r}_{m,yx}^{(3)} \mathbf{Z}_y^{(1)} \mathbf{Z}_x^{(2)} \mathbf{Z}_x^{(3)} \boldsymbol{\mu} + \frac{\partial^3 w_p}{\partial y \partial x^2} \quad (\text{B.17})$$

where $\mathbf{Z}_x^{(3)} = \begin{bmatrix} -2 & -1 \cdots (m-2) & -1 & 0 \cdots (m-2) \end{bmatrix}$ and $\mathbf{Z}_y^{(3)} = \begin{bmatrix} 2 & 1 \cdots -(m-2) & -1 & 0 \cdots -(m-2) \end{bmatrix}$.

Further

$$\mathbf{r}_{m,x}^{(3)} = [P_{-3} \cdots P_{m-3} \ Q_{-2} \cdots Q_{m-3}] \quad (\text{B.18})$$

$$\mathbf{r}_{m,y}^{(3)} = [Q_{-3} \cdots Q_{m-3} \ P_{-2} \cdots P_{m-3}] \quad (\text{B.19})$$

while $\mathbf{r}_{m,xy}^{(3)} = \mathbf{r}_{m,x}^{(3)}$ and $\mathbf{r}_{m,yx}^{(3)} = \mathbf{r}_{m,y}^{(3)}$

In this manner, taking into account Eqs. (2) and (3) and manipulating yields the bending and twisting moments as

$$M_x = -D \left[\left(\mathbf{r}_{m,x}^{(2)} \mathbf{Z}_x^{(1)} \mathbf{Z}_x^{(2)} + \nu \mathbf{r}_{m,y}^{(2)} \mathbf{Z}_y^{(1)} \mathbf{Z}_y^{(2)} \right) \boldsymbol{\mu} + \left(\frac{\partial^2 w_p}{\partial x^2} + \nu \frac{\partial^2 w_p}{\partial y^2} \right) \right] \quad (\text{B.20})$$

$$M_y = -D \left[\left(\mathbf{r}_{m,y}^{(2)} \mathbf{Z}_y^{(1)} \mathbf{Z}_y^{(2)} + \nu \mathbf{r}_{m,x}^{(2)} \mathbf{Z}_x^{(1)} \mathbf{Z}_x^{(2)} \right) \boldsymbol{\mu} + \left(\frac{\partial^2 w_p}{\partial y^2} + \nu \frac{\partial^2 w_p}{\partial x^2} \right) \right] \quad (\text{B.21})$$

$$M_{xy} = -D(1-\nu) \left(\mathbf{r}_{m,xy}^{(2)} \mathbf{Z}_y^{(1)} \mathbf{Z}_x^{(2)} \boldsymbol{\mu} + \frac{\partial^2 w_p}{\partial x \partial y} \right) \quad (\text{B.22})$$

while the shearing forces are given as

$$V_x = -D \left[\left(\mathbf{r}_{m,x}^{(3)} \mathbf{Z}_x^{(1)} \mathbf{Z}_x^{(2)} \mathbf{Z}_x^{(3)} + \mathbf{r}_{m,xy}^{(3)} \mathbf{Z}_x^{(1)} \mathbf{Z}_y^{(2)} \mathbf{Z}_y^{(3)} \right) \boldsymbol{\mu} + \left(\frac{\partial^3 w_p}{\partial x^3} + \frac{\partial^3 w_p}{\partial x \partial y^2} \right) \right] \quad (\text{B.23})$$

$$V_y = -D \left[\left(\mathbf{r}_{m,y}^{(3)} \mathbf{Z}_y^{(1)} \mathbf{Z}_y^{(2)} \mathbf{Z}_y^{(3)} + \mathbf{r}_{m,yx}^{(3)} \mathbf{Z}_y^{(1)} \mathbf{Z}_x^{(2)} \mathbf{Z}_x^{(3)} \right) \boldsymbol{\mu} + \left(\frac{\partial^3 w_p}{\partial y^3} + \frac{\partial^3 w_p}{\partial y \partial x^2} \right) \right] \quad (\text{B.24})$$

Further, normal stresses σ_x and σ_y , given as

$$\sigma_x = -\frac{Ez}{1-\nu^2} \left(\frac{\partial^2 w}{\partial x^2} + \nu \frac{\partial^2 w}{\partial y^2} \right) \quad (\text{B.25})$$

and

$$\sigma_y = -\frac{Ez}{1-\nu^2} \left(\frac{\partial^2 w}{\partial y^2} + \nu \frac{\partial^2 w}{\partial x^2} \right) \quad (\text{B.26})$$

can be directly expressed as

$$\sigma_x = -\frac{Ez}{1-\nu^2} \left[\left(\mathbf{r}_{m,x}^{(2)} \mathbf{Z}_x^{(1)} \mathbf{Z}_x^{(2)} + \nu \mathbf{r}_{m,y}^{(2)} \mathbf{Z}_y^{(1)} \mathbf{Z}_y^{(2)} \right) \boldsymbol{\mu} + \left(\frac{\partial^2 w_p}{\partial x^2} + \nu \frac{\partial^2 w_p}{\partial y^2} \right) \right] \quad (\text{B.27})$$

and

$$\sigma_y = -\frac{Ez}{1-\nu^2} \left[\left(\mathbf{r}_{m,y}^{(2)} \mathbf{Z}_y^{(1)} \mathbf{Z}_y^{(2)} + \nu \mathbf{r}_{m,x}^{(2)} \mathbf{Z}_x^{(1)} \mathbf{Z}_x^{(2)} \right) \boldsymbol{\mu} + \left(\frac{\partial^2 w_p}{\partial y^2} + \nu \frac{\partial^2 w_p}{\partial x^2} \right) \right] \quad (\text{B.28})$$

Similarly, shear stresses τ

$$\tau = -\frac{E}{1+\nu} \left(\frac{\partial^2 w}{\partial x \partial y} z \right) \quad (\text{B.29})$$

can be given as

$$\tau = -\frac{E}{1+\nu} z \left[\mathbf{r}_{m,xy}^{(2)} \mathbf{Z}_y^{(1)} \mathbf{Z}_x^{(2)} \boldsymbol{\mu} + \frac{\partial^2 w_p}{\partial x \partial y} \right] \quad (\text{B.30})$$

Note that Eqs. (B.3), (B.4), (B.20)-(B.24) are then useful to directly express the BCs in Eqs. (6)-(12) in terms of harmonic polynomials. These expressions can be then used in the functionals in Eqs. (60)-(62).

References

- [1] SP Timoshenko, S Woinowsky-Krieger, Theory of plates and shells. McGraw-Hill, New York, 1959.
- [2] AM Zenkour, Bending of thin rectangular plates with variable-thickness in a hygrothermal environment, *Thin-Walled Struct.* 123 (2018) 333-340.
- [3] A Reali, H Gomez, A modified Kirchhoff plate theory for analyzing thermo-mechanical static and buckling responses of functionally graded material plates, *Thin-Walled Struct.* 117 (2017) 113-126.
- [4] F Maurin, F Greco, L Coox, D Vandepitte, W Desmet, Isogeometric collocation for Kirchhoff-Love plates and shells, *Comput Meth Appl Mech Eng.* 329 (2018) 396-420.
- [5] OC Zienkiewicz, The finite element method in engineering science. McGraw-Hill, New York, 1984.
- [6] JT Katsikadelis, The Boundary Element Method for Engineers and Scientists, Second Edition: Theory and Applications. Academic Press, London, 2016.
- [7] GR Liu, Meshfree Methods: Moving Beyond the Finite Element Method. CRC Press, Boca Raton, 2010.
- [8] S Li, WK Liu, Meshfree and particle methods and their applications, *Appl Mech Rev* 55 (2002) 1-34.
- [9] JS Chen, M Hillman, SW Chi, Meshfree methods: progress made after 20 years, *J Eng Mech.* 143 (2017) [https://doi.org/10.1061/\(ASCE\)EM.1943-7889.0001176](https://doi.org/10.1061/(ASCE)EM.1943-7889.0001176).
- [10] S Çeribaşı, G Altay, MC Dökmeçi, Static analysis of superelliptical clamped plates by Galerkin's method, *Thin-Walled Struct.* 46 (2008) 122-127.
- [11] T Belytschko, D Organ, Y Krongauz, A coupled finite element–element-free Galerkin method, *Comput Mech.* 17 (1995) 186-195.
- [12] SN Atluri, T Zhu, New concepts in meshless methods, *Int J Num Meth Eng.* 47 (2000) 537–556.
- [13] CA Duarte, JT Oden, An hp adaptive method using clouds, *Comput Meth Appl Mech Eng.* 139 (1996) 237–262.
- [14] L Chen, YM Cheng, HP Ma, The complex variable reproducing kernel particle method for the analysis of Kirchhoff plates, *Comput Mech.* 55 (2015) 591-602.
- [15] S Sadamoto, S Tanaka, K Taniguchi, M Ozdemir, TQ Bui, C Murakami, D Yanagihara, Buckling analysis of stiffened plate structures by an improved meshfree flat shell formulation, *Thin-Walled Struct.* 117 (2017) 303-313.

- [16] VMA Leitao, A meshless method for Kirchhoff plate bending problems, *Int J Num Meth Eng.* 52 (2001) 1107-1130.
- [17] S Sadamoto, M Ozdemir, S Tanaka, K Taniguchi, TT Yu, TQ Bui, An effective meshfree reproducing kernel method for buckling analysis of cylindrical shells with and without cutouts, *Comput Mech.* 59 (2017) 919-932.
- [18] CH Thai, TN Nguyen, T Rabczuk, H Nguyen-Xuan, An improved moving Kriging meshfree method for plate analysis using a refined plate theory, *Comput Struct.* 176 (2016) 34-49.
- [19] M Bitaraf, S Mohammadi, Large deflection analysis of flexible plates by the meshless finite point method, *Thin-Walled Struct.* 48 (2010) 200-214.
- [20] CH Thai, AJM Ferreira, H Nguyen-Xuan, Naturally stabilized nodal integration meshfree formulations for analysis of laminated composite and sandwich plates, *Compos Struct.* 178 (2017) 260-276.
- [21] Y Liu, YC Hon, LM Liew, A meshfree Hermite-type radial point interpolation method for Kirchhoff plate problems, *Int J Num Meth Eng.* 66 (2006) 1153-1178.
- [22] TQ Bui, MN Nguyen, Ch Zhang, Buckling analysis of Reissner–Mindlin plates subjected to in-plane edge loads using a shear-locking-free and meshfree method, *Eng Anal Bound Elem.* 35 (2011) 1038-1053.
- [23] WG Jin, YK Cheung, OC Zienkiewicz, Trefftz method for Kirchhoff plate bending problems, *Int J Num Meth Eng.* 36 (1993) 765-781.
- [24] KM Liew, CM Wang, pb-2 Rayleigh-Ritz method for general plate analysis, *Eng Struct.* 15 (1993) 55-60.
- [25] G Battaglia, A Di Matteo, G Micale, A Pirrotta, Vibration-based identification of mechanical properties of orthotropic arbitrarily shaped plates: Numerical and experimental assessment, *Compos. Pt. B-Eng.* 150 (2018) 212-225.
- [26] MM Saadatpou, M Azhari, The Galerkin method for static analysis of simply supported plates of general shape, *Comput Struct.* 69 (1998) 1-9.
- [27] M Di Paola, A Pirrotta, R Santoro, Line Element-less Method (LEM) for beam torsion solution (Truly no-mesh method), *Acta Mech.* 195 (2008) 349-63.
- [28] M Di Paola, A Pirrotta, R Santoro, De Saint-Venant flexure-torsion problem handled by Line Element-less Method (LEM), *Acta Mech.* 217 (2011) 101-118.
- [29] A Pirrotta, LEM for twisted re-entrant angle sections. *Comput Struct.* 133 (2014) 149-155.
- [30] R Santoro, The Line Element-less Method analysis of orthotropic beam for the De Saint Venant torsion problem, *Int J Mech Sci.* 52 (2010) 43–55.

- [31] R Santoro, Solution of de Saint Venant flexure-torsion problem for orthotropic beam via LEM (Line Element-less Method), *Eur J Mech A-Solids*, 30 (2011) 924-939.
- [32] E Murtha-Smith, Plate analogy for the torsion problem, *J Eng Mech*. 116 (1990) 1-17.
- [33] H Irschik, Analogies between bending of plates and torsion problem, *J Eng Mech*. 117 (1991) 2503-2508.
- [34] R Barretta, Analogies between Kirchhoff plates and Saint-Venant beams, *Acta Mech*. 224 (2013) 2955-2964.
- [35] A Pirrotta, C Bucher, Innovative straight formulation for plate in bending, *Comput Struct*. 180 (2017) 117-124.
- [36] R Szilard, *Theories and Applications of Plate Analysis: Classical, Numerical and Engineering Methods*. John Wiley & Sons, Hoboken, 2004.
- [37] H Marcus, *Die Theorie elastischer Gewebe und ihre Anwendung auf die Berechnung biegsamer Platten*. Springer, Berlin, 1924.
- [38] E Ventsel, T Krauthammer, *Thin plates and shells: Theory, analysis, and applications*. CRC Press, New York, 2001.
- [39] KM Liew, YQ Huang, JN Reddy, Analysis of general shaped thin plates by the moving least-squares differential quadrature method, *Finite Elem Anal Des*. 40 (2004) 1453-1474.
- [40] KM Liew, FL Liu, Differential cubature method: A solution technique for Kirchhoff plates of arbitrary shape, *Comput Meth Appl Mech Eng*. 145 (1997) 1-10.
- [41] CS Chen, AS Muleshkov, MA Golberg, The numerical evaluation of particular solutions for Poisson's equation - a revisit. *Trans Model Simul*. 24 (1999) <https://doi.org/10.2495/BE990281>.
- [42] MA Golberg, AS Muleshkov, CS Chen, AHD Cheng, Polynomial particular solutions for certain partial differential operators, *Numer Meth Part Differ Equ*. 19 (2003) 112-133.
- [43] M Abramowitz, IA Stegun, *Handbook of Mathematical Functions: with Formulas, Graphs, and Mathematical Tables*. Dover, New York, 1972.